Efficient wave tank assessment of WEC performance

Giorgio Bacelli
Sandia National Labs
Albuquerque, NM, USA

Steven J, Spencer
Sandia National Labs
Albuquerque, NM, USA

Ryan G. Coe*
Sandia National Labs
Albuquerque, NM, USA

*Corresponding author: rcoe@sandia.gov

1. INTRODUCTION

Wave tank testing of wave energy converters (WECs) is generally undertaken for one of two reasons: numerical model identification/validation or performance evaluation. In the case of performance evaluation, some aspect(s) of WEC performance, such as power absorption, power generation, or loading is assessed using an experimental device. With a large number of performance assessment experiments being conducted on various devices, it is key that the design of experiments be such as to maximize cost efficiency. Advanced control of the power take-off (PTO) in a WEC has shown significant promise for increasing wave energy absorption in simulation [1, 2]. The tuning of control strategies, which should be performed numerically to the extent possible, adds another factor to assessing WEC performance in wave tank testing.

A $1/17^{th}$ scale WEC device has been designed for tests concerned with the study of WEC modeling and control [3, 4]. Figure 1 and Table 1 show a diagram of the WEC device and its relevant physical parameters. A detailed description of the basin and how the WEC device was tested within the basin (i.e., installation, location, mounting) is given in [3]. The WEC is capable of moving in three degrees of freedom (heave, pitch, and surge) to allow for full motion in a single plane. Each degree of freedom is actuated independently. In addition, a series of large springs are used to provide a restoring force in surge. The inclusion of the springs in the design was chosen to improve the safety of the system. Since there is no hydrostatic restoring reaction in surge, an instability or error in the actuator system (or even a loss of power during a wave tests) could otherwise cause damage to the system.

For this study, we consider a JONSWAP sea state with $H_s = 0.127$ m, $T_p = 3.5$ s, and $\gamma = 3.3$. First, the concept of short repeat period wave trains for performance assessment is considered. Next, a matrix of proportional and integral control gains (i.e., P and PI controllers, see, e.g., [5]) are evaluated in the wave tank.
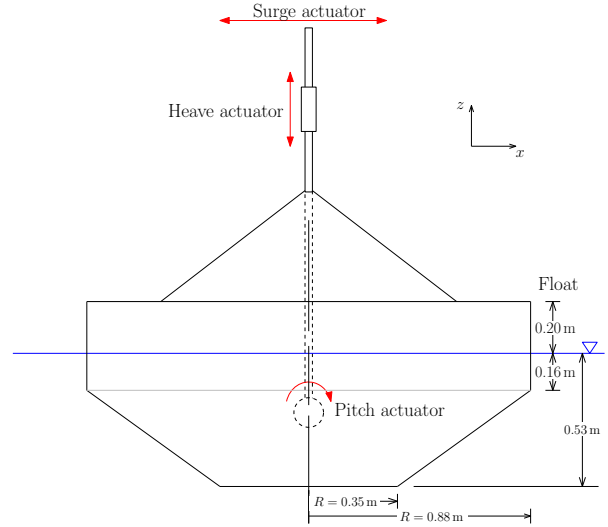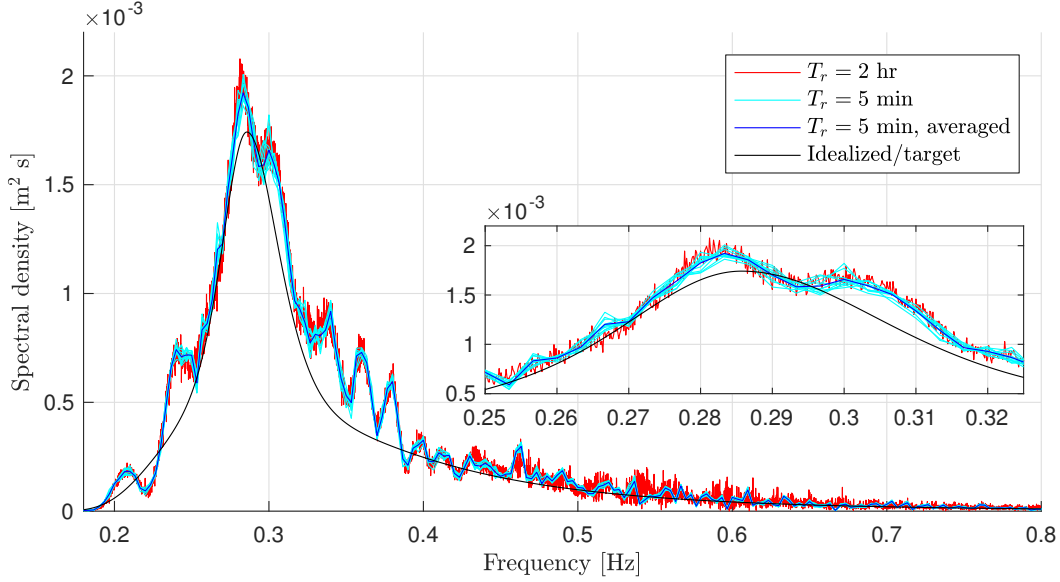

Figure 1: Test device diagram.

2. METHODS

As detailed in previous work on system identification (SID) of WECs [6], there are many advantages to utilizing periodic signals when working with WECs. Based on this, it is desirable also to use periodic (repeating) wave signals when assessing WEC control performance. To ensure the validity of this approach, two tests were conducted to provide a comparison of spectral energy. First, a two hour test was run using a wave signal with two hour repeat period ($T_r = 2$ hr). Second, the same wave spectrum was run using a 5 minute repeat period ($T_r = 5$ min). This second test was run for 60 minutes (12 periods). The results of this test are shown in Figure 2 for a JONSWAP spectrum with a significant wave height of $H_s = 0.127$ m, a peak period of $T_p = 3.5$ s, and a peakedness factor of $\gamma = 3.3$. Note that for the case of $T_r = 5$ min, Figure 2 shows the spectrum from each of the 12 periods in the test individually, and averaged over all the 12 periods. Periodic signals provide benefits also when processing data; in fact, all the plots in Figure 2 have been obtained by simply extracting a number of samples from the time series corresponding to an integer number of periods, and taking the discrete Fourier

Figure 2: Comparison of target (idealized), measured pseudo-random, and measured periodic wave spectra for the test sea state. The plot contains a detailed inset of the spectra for $0.25 \leq f \leq 0.325$.

Table 1: Model-scale WEC physical parameters.

Parameter	Value
Rigid-body mass (float & slider), m [kg]	858
Displaced volume, $\forall$ [m³]	0.858
Float radius, r [m]	0.88
Float draft, T [m]	0.53
Water density, ρ [kg/m³]	1000
Water depth, h [m]	6.1
Linear hydrostatic stiffness, G [kN/m]	23.9
Infinite-frequency added mass, A_∞ [kg]	822
Max vertical travel, $|z_\mathrm{max}|$ [m]	0.6

transform (using the FFT algorithm). No filtering, windowing or other manipulation has been applied to the data. For example, if the sampling frequency is 1kHz and the period is $T_r = 300s$, the number of samples per period is $N = 3 \times 10^5$.

From Figure 2, we can see that the spectra from the two experimental tests (pseudo-random and periodic) overlap each other closely. While there is higher fidelity frequency resolution in the $T_r = 2\,\mathrm{hr}$ test, the frequency resolution of the periodic test is easily sufficient to capture the target spectrum. Table 2 provides the spectral moments of interest, defined for a spectral density $S(\omega)$ as

$$m_n = \int \omega^n S(\omega)\, d\omega. \tag{1}$$

Additionally, the average wave energy transport (also sometimes referred to as the wave energy flux), given by

$$J = \rho g \int c_g S(\omega)\, d\omega, \tag{2}$$

is shown in Table 2. Here, c_g is the group velocity, which is the velocity at which wave energy is transported. This can be defined in terms of the phase velocity, c_p, for water of arbitrary depth as

$$c_g = \left(\frac{1}{2} + \frac{kh}{\sinh\left(2kh\right)} \right) c_p \tag{3}$$

Here, h is the water depth (from Table 1, the MASK basin has a depth of $h = 6.1\,\mathrm{m}$). In deep water, Eqn. (3) can be reduced to show the group velocity is half the phase velocity ($c_g = c_p/2$). The phase velocity is defined by the ratio of the frequency, ω, to the wave number, k.

$$c_p = \frac{\omega}{k} \tag{4}$$

The wave number is inversely related to the wave length ($k = 2\pi/\lambda$). The wave number and frequency are related to each other by the dispersion relation.

$$\omega^2 = gk \tanh\left(kh\right) \tag{5}$$

Excellent in-depth derivations and discussions on surface waves are available from a number of sources (see, e.g., [7, 8]).

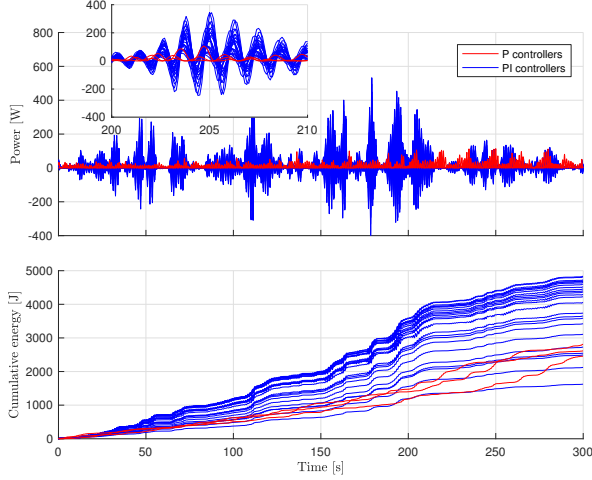From Table 2, it is clear that the $T_r = 2\,\mathrm{hr}$ and $T_r = 5\,\mathrm{min}$ waves match each other closely. While there is indeed some error between the measured spectra and the idealize/target spectrum, this is not a concern in this case, as study is concerned with relative performance (not matching some exact ocean condition). With the evidence that 5 minute repeat periods are spectrally equivalent to much longer tests, it is possible to efficiently consider a large matrix of control gains.

3. RESULTS

Figure 3-5 show sample results from a test comparing a range of proportional and integral gains in the

Table 2: Moments from idealized/target, measured pseudo-random, and measured periodic wave spectra for the test sea state.

Wave realization	$m_0 \times 10^{-3}$ [m²]	$m_1 \times 10^{-3}$ [m²/s]	$m_2 \times 10^{-3}$ [m²/s²]	J [w/m]
$T_r = 2\,\mathrm{hr}$	0.1952	0.0666	0.0250	31.96
$T_r = 5\,\mathrm{min}$	0.1944	0.0660	0.0246	31.94
Idealized/target	0.1596	0.0538	0.0199	26.48

Figure 3: Power absorption over time from the test sea state with P (red) and PI (blue) controllers at difference gains.

test sea state. While effectively comparing 25 different gain settings for the controller, this test only took just over 2 h; a significant improvement compared to tests run with unnecessarily long repeat periods. As discussed in Section 2, each gain setting is evaluated for five minutes. Figure 3 shows both the instantaneous power and the cumulative absorbed energy over time for each controller. An inset plot for $200 \le t \le 210\,\mathrm{s}$ is included in Figure 3 to highlight how the instantaneous power varies for each controller. It is clear to see that the different gains perform quite similarly. A frequency domain comparison of the same experiments is shown in Figure 4, which shows the average absorbed power at each frequency component for different values of the controllers' parameters.

Figure 5 shows the estimated values of the controller gains; estimation of these parameters have been carried out in both time and frequency, confirming that the actuator system is capable of implementing the control signal requested by control algorithms. The upper plot shows the proportional gain estimation, in both the time and frequency domain (left and right, respectively). Likewise, estimates for the integral gain are shown in the lower half of Figure 5. In the time domain, the stiffness and damping coefficients, k_I and k_P, are obtained by using the least squares method to find an approximate solution to the overdetermined linear system of equa-

tions:

$$
\begin{bmatrix} z_1 & v_1 \\ z_2 & v_2 \\ \cdots & \cdots \\ z_N & v_N \end{bmatrix} \begin{bmatrix} k_I \\ k_P \end{bmatrix} = \begin{bmatrix} f_1 \\ f_2 \\ \cdots \\ f_N \end{bmatrix}, \tag{6}
$$

where z_i, v_i, f_i are, respectively, the i-th samples of the position, velocity and PTO force. The parameter estimation in the frequency domain is carried out by trimming the time series of the force and velocity in sets containing a number of samples corresponding to 300 s, that is the length of the repeating period for which the parameters k_I and k_P are held constant. The stiffness and damping coefficients are then calculated by taking the discrete Fourier transform (i.e., FFT) of both force and velocity, and calculating the PTO impedance, Z_{PTO} defined as:

$$
Z_{PTO}(\omega) = k_P + i\frac{k_I}{\omega} = \frac{F(\omega)}{V(\omega)}. \tag{7}
$$

From the PTO impedance, the damping coefficient k_P can be extracted as the real part of Z_{PTO}, while the stiffness coefficient is the imaginary part of the PTO impedance multiplied by the angular frequency, i.e.:

$$
k_p = \mathrm{Re}[Z_{PTO}] \tag{8}
$$
$$
k_I = \omega\,\mathrm{Im}[Z_{PTO}]. \tag{9}
$$

Figure 6 shows the average absorbed power as function of the controller gains in the test sea state. The maximum average power obtained was 16 W, using $k_P = 1.5\,\mathrm{kN\text{-}s/m}$ and $k_I = -14\,\mathrm{kN/m}$. From Figure 6, we can see that the optimal damping, k_P, is largest for small magnitudes of reactive control. For instance, with $k_I = -2.0\,\mathrm{kN/m}$, the damping gain which produces the maximum power is $k_P^{\max} \ge 3.0\,\mathrm{kN\text{-}s/m}$. As k_I is increased, $k_P^{\max}$ decreases; at the largest magnitude of reactive power tested ($k_I = -16\,\mathrm{kN/m}$), we can see that $k_P^{\max} \le 1.0\,\mathrm{kN\text{-}s/m}$.

4. ACKNOWLEDGEMENTS

5. REFERENCES

[1] Hals, J., Falnes, J., and Moan, T., 2011. "A comparison of selected strategies for adaptive control of wave energy converters". *Journal of Offshore Mechanics and Arctic Engineering*, **133**(3), March, p. 031101.
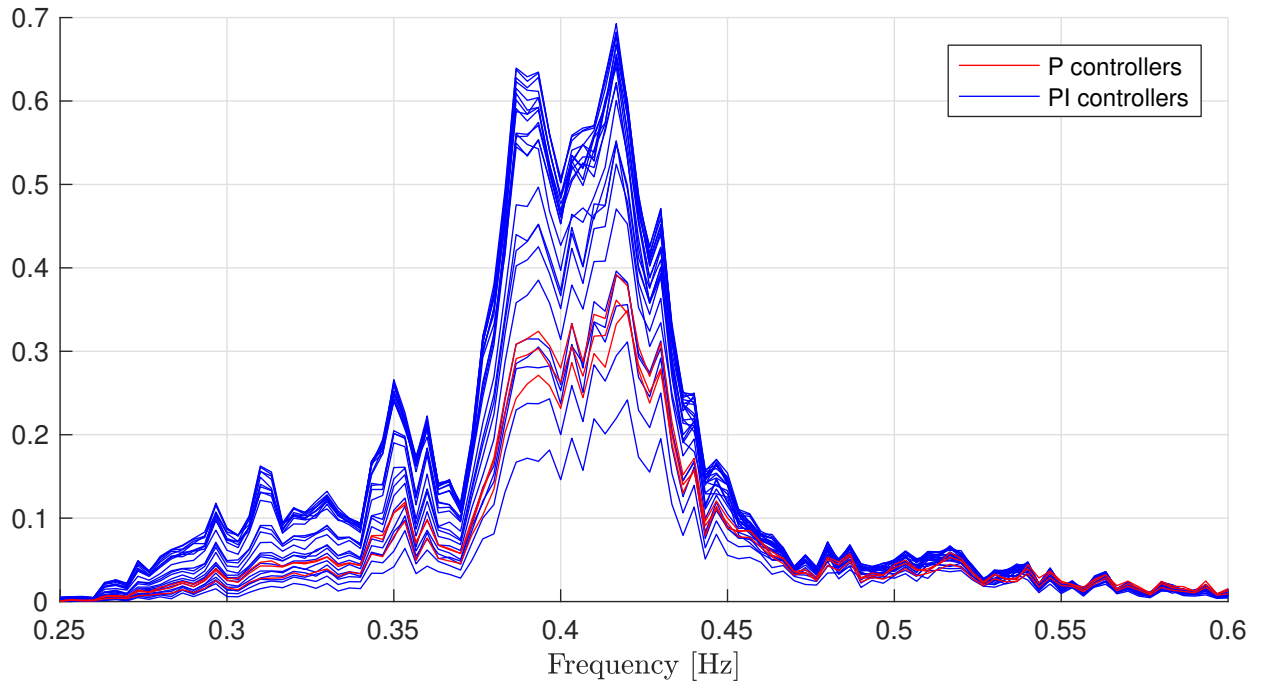
Figure 4: Fourier analysis of power absorption with P (red) and PI (blue) controllers at difference gains.
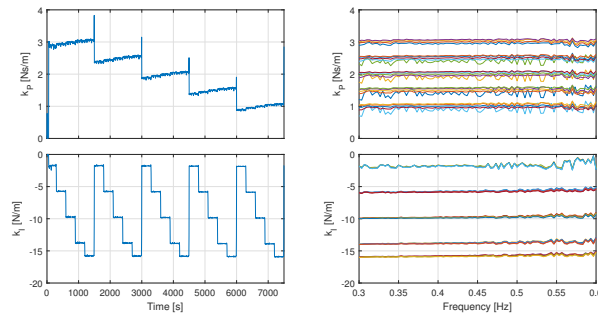

Figure 5: Estimated damping and stiffness coefficients from the test sea state, both in time and frequency domain.
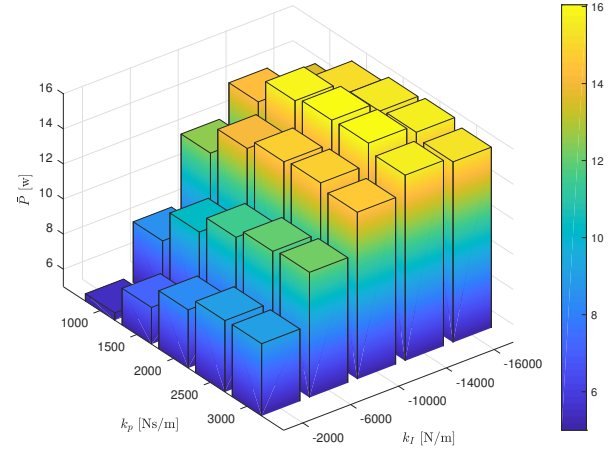

Figure 6: Test matrix from the test sea state with varying PI control (color bar shows average power).

[2] Coe, R. G., Bacelli, G., Wilson, D. G., Abdelkhalik, O., Korde, U. A., and III, R. D. R., 2017. "A comparison of control strategies for wave energy converters". *International Journal of Marine Energy,* **20**(Supplement C), pp. 45 – 63.

[3] Coe, R. G., Bacelli, G., Patterson, D., and Wilson, D. G., 2016. Advanced WEC Dynamics & Controls FY16 testing report. Tech. Rep. SAND2016-10094, Sandia National Labs, Albuquerque, NM, October.

[4] Bacelli, G., Spencer, S. J., Coe, R. G., Mazumdar, A., Patterson, D., and Dullea, K., 2017. "Design and bench testing of a model-scale WEC for advanced PTO control research". In European Wave and Tidal Energy Conference (EWTEC).

[5] Ogata, K., 2002. *Modern Control Engineering.* Prentice Hall.

[6] Bacelli, G., Coe, R. G., Patterson, D., and Wilson, D., 2017. "System identification of a heaving point absorber: Design of experiment and device modeling". *Energies,* **10**(10), p. 472.

[7] Newman, J. N., 1978. *Marine hydrodynamics.* MIT Press, Cambridge, Massachusetts.

[8] Falnes, J., 2002. *Ocean Waves and Oscillating Systems.* Cambridge University Press, Cambridge; New York.